



Investigation of the workability and surface roughness of thin brass wires in various dieless drawing technologies

Andrij Milenin¹ · Mirosław Wróbel¹ · Piotr Kustra^{1,2}

Received: 8 July 2021 / Revised: 20 October 2021 / Accepted: 30 October 2021 / Published online: 16 November 2021
© The Author(s) 2021

Abstract

Possibilities of improving the workability of the CuZn37 brass thin wire in a diameter of 0.14–0.18 mm produced by the dieless drawing processes were explored. The workability was defined as the maximum final longitudinal strain of the wire up to its fracture, achievable in the dieless drawing process. Two technologies of dieless drawing were developed and their workability was compared. The first one is the classical one-pass process; the second, a multi-pass one. For both developed technologies, it was possible to obtain a good-quality product but more than two times higher workability has been demonstrated for the multi-pass technology. No evident effect of the deformation temperature from the window of technologically accepted parameters on the workability was found but an increase in the temperature significantly increased the roughness of the product surface. For the same deformation temperature, the roughness of the wire obtained from the multi-pass process appeared to be significantly lower than for the one of the classical one-pass technologies.

Keywords Dieless drawing · Thin wire · Brass · Workability · Roughness

1 Introduction

Thin wires made of copper-based alloys are widely used in the industry, robotic, filtration, etc. Beyond this, thin brass wires are commonly used as the electrically charged wires in electric discharge machining [1] and jewelry manufacturing [2]. The conventional manufacturing technology of thin brass wire is based on a drawing in dies with diamond cores. The use of a die significantly increases the cost of the process. On the other hand, conventional wire drawing technology requires the use of some lubricants, and their removal from the final product by chemical treatment degrades the surface quality and is not harmless to the natural environment. Thus, this technology is quite expensive [3].

The dieless drawing (DD) technology can provide solutions to the above problems. The DD process is based on a wire or tube stretching with simultaneous local heating of the deformation zone. The heated zone moves along the

deformed product. An electric furnace, inductor, or laser is usually used as the heat source. To the best of our knowledge, DD technology was invented by Weiss and Kot [4]. DD enables to obtain a product with a variable cross-sectional shape and size of the product along its length [5], which is impossible to obtain with conventional drawing or extrusion. Also, DD can be used in conjunction with conventional wire drawing [6].

High productivity due to a relatively large possible cross-section reduction in a single pass is a significant advantage of this technology. An investigation of this problem was a motivation for our study. The workability of the material is defined as the maximum final cross-section reduction (or longitudinal strain) of the wire up to its fracture achievable in the DD process. Up to 72% in the cross-section reduction of the single-pass was successfully applied by Tiernan and Hillery [7] during DD of a carbon steel wire. In the case of a commercial-grade nickel, the workability significantly increases when the process is conducted in an inert gas atmosphere and the single-pass maximum reduction in the area can reach 30–40% [8]. Such workability is possible due to the high temperature in the deformation zone and the absence of friction between the die and the wire. This technology allows the production of a very thin wire, in diameter limited by the precision of the process parameters control.

✉ Piotr Kustra
pkustra@agh.edu.pl

¹ Faculty of Metals Engineering and Industrial Computer Science, AGH University of Science and Technology, al. Mickiewicza 30, 30-059 Kraków, Poland

² ul. Czarnowiejska 66, 30-054 Kraków, Poland

E.g. Li et al. [8] reported the development of a laser dieless drawing (LDD) technology for a commercial-grade nickel wire with diameters of 0.125–0.5 mm. Potentially, DD may allow obtaining a wire with a much smaller diameter but two important problems must be solved.

The first one is the optimal choice of process parameters to achieve maximum stability of deformation in the deformation zone and, consequently, high workability and uniformity of the diameter along the length of the processed wire. One of the possible solutions to this problem was proposed in work [9] for LDD of tubes, made from magnesium alloy. The idea behind this approach is to perform multi-pass dieless drawing (MPDD) with small increments of strain in each pass, which slows down the formation of the neck in the deformed material and, in consequence, improves workability. This approach reduces diameter unevenness along the length of the wire and improves the workability of the material in the MPDD process.

By the effectiveness (E) of the MPDD process, we mean the ratio of the workability in multi-pass deformation to this value obtained by a single-pass conventional DD process. The effectiveness of MPDD depends on the stability of plastic deformation in the deformation zone, which is related to the sensitivity of the flow stress of the deformable material to strain, strain rate, and temperature. With the high stability of plastic deformation, the MPDD method becomes more efficient. As a basis for numerical estimation of stability of plastic deformation during DD and MPDD, the Considère criterion [10] can be used in the form of an equation:

$$\sigma = \frac{d\sigma}{d\varepsilon}, \quad (1)$$

where σ flow stress and ε effective strain.

The criterion has been used frequently in the literature, also for a complex stress–strain state deformation [11], and sometimes is expressed in the form of the following parameter K [12]:

$$K = \frac{d\sigma}{d\varepsilon} \frac{1}{\sigma}, \quad (2)$$

Since the flow stress σ depends on temperature t , effective strain ε and strain rate ξ , Eq. (1) can be expressed as [13]

$$\sigma = \frac{d\sigma}{d\varepsilon} = \frac{\partial\sigma}{\partial t} \frac{\partial t}{\partial\varepsilon} + \frac{\partial\sigma}{\partial\xi} \frac{\partial\xi}{\partial\varepsilon} + \frac{\partial\sigma}{\partial\varepsilon}. \quad (3)$$

For DD, Eq. (3) was also applied by Li [14]. According to He et al. [15], direct use of the Eqs. (1–3) for DD usually does not lead to success, and based on their paper, experimentally determined maps of the stable processing limit parameters are recommended. In our opinion, the Considère criterion can be used with caution for the DD process, provided that the stress and strain states are correctly

determined. Thus, this criterion can be directly implemented in the Finite Elements (FE) model of DD similarly as was earlier proposed and tested in work [16].

As follows from Eq. (3), one of the possibilities of improving the stability of deformation in the DD processes is to increase $\partial\sigma/\partial t$ by rapidly cooling the material behind the deformation zone. The local increase in the wire temperature should locally start the plastic deformation and then the cooling of the deformed material after it leaves the deformation zone should stop the deformation due to an increase in the flow stress when the temperature decreases. The rapid cooling DD was described in the literature (e.g. Ref. [17]).

For linear stretching, $K < 1$ corresponds to the condition when the process of plastic deformation becomes unstable. In the process of DD, the cooling of the material after leaving the heating zone is a factor that further stabilizes the process. This leads to the increased flow stress corresponding to cooling ceasing the initiated strain instability. Therefore, the DD process is usually more stable than linear stretching at a uniformly distributed temperature in the sample.

The loss of stability and the subsequent localization of the deformation is a stage preceding the fracture of the material during DD of sufficiently ductile materials. In this case, the fracture mechanism limiting the workability of the material in DD is based on necking in the deformation zone. Another mechanism is the exhaustion of the ductility limit, which is typical for low ductile materials, such as some magnesium alloys. In the case of highly ductile materials (or a properly selected heating temperature, which makes the material highly ductile), the deformation conditions can be chosen so that the value of the stability parameter is high. This will allow avoiding early necking and, as a result, will improve the workability of the materials in the DD process. Such conditions can be achieved in the MPDD process by reducing the strain increment and repeating the process several times. This approach works best when heating the wire in every pass leads to a complete or at least partial restoration of the mechanical properties of the deformed material [16].

Thus, it can be concluded that the conditions for the occurrence of instability of deformation and material fracture during DD have been well studied. Moreover, the MPDD method was proposed for improving the workability due to the deformation of the material at high values of the stability parameter (2). This is achieved through the use of the MPDD, which makes it possible to divide the process into many small steps, in each of which a high value of the parameter (2) is achieved and the mechanical properties of the material are fully or partially restored. However, the efficiency of the MPDD process is strongly dependent on the rheological parameters of the material. Thus, the processing of a new material requires an investigation of the sensitivity of the flow stress to strain and the strain rate at different temperatures. On the other hand, the choice of the

deformation temperature is also extremely important. Overheating can lead to intense oxidation and high-temperature fracture of copper-based alloys [18], underheating can lead to low ductility.

In the present study, a methodology of a multi-pass MPDD was successfully developed for CuZn37 brass wire and applied for thin wire manufacturing. Estimating the gain in the workability of the deformation process was the main goal of the present work. Selection of optimal parameters maximizing the workability of the CuZn37 brass wire with a diameter in the range of 0.14–0.18 mm was the operational goal of our work.

When searching for the optimal technology offering the maximum workability, we have to keep in mind that some combinations of parameters can deteriorate the surface roughness of the product. The surface roughness is an important problem of the thin wire technology, which decides about the quality of products. Therefore, an investigation of the surface roughness was the second objective of the present work.

An increase in the roughness results both from the strain and oxidation. The strain effect on roughness was reported by Furushima and Manabe [19] and identified as a source of decrease in the DD workability [20]. The reason for the appearance of the strain-induced roughness is the inhomogeneity of the mechanical properties of the material, caused, as a rule, by the crystallographic texture and grain structure of the material. That is why the study of texture and microstructure was also necessary to explain the strain-induced roughness changes. The roughness problem was a subject of our previous study by theoretical [21] and experimental [22]

methods, but an effect of MPDD on the product roughness has been omitted in the literature. Thus, this effect was a part of the present study.

2 Materials and methods

2.1 Materials

A commercial cold-drawn CuZn37 brass wire, in a diameter of 0.2 mm (d_0), was used as a workpiece. The metallographic microscope Axio Imager M1m by ZEISS and the scanning electron microscope (SEM) Inspect S50 by FEI were used for the microstructure characterization. The optical profiler Wyko NT930 by Veeco was used for surface roughness measurements.

The crystallographic texture orientation distribution function (ODF) was calculated by a commercial LaboTex software [23] for a set of incomplete pole Figs. 111, 200, 220, and 311 measured on the Panalytical Emperyan diffractometer by the Schulz reflection methodology [24]. The lack of sample symmetry and cubic crystal symmetry was assumed in the calculations.

The wire had [111] fiber texture, typical for the drawn wires (Fig. 1), the grains were elongated in the wire axis what is typical for highly deformed materials (Fig. 2a), and the wire surface was covered with clear traces of the tool (Fig. 2b). The surface roughness R_a was equal to 0.12 μm (Fig. 3). Some duplex fiber textures of [111] and [100] orientations are usually developed in brass deformed by wire drawing and the first of them is usually much stronger [25].

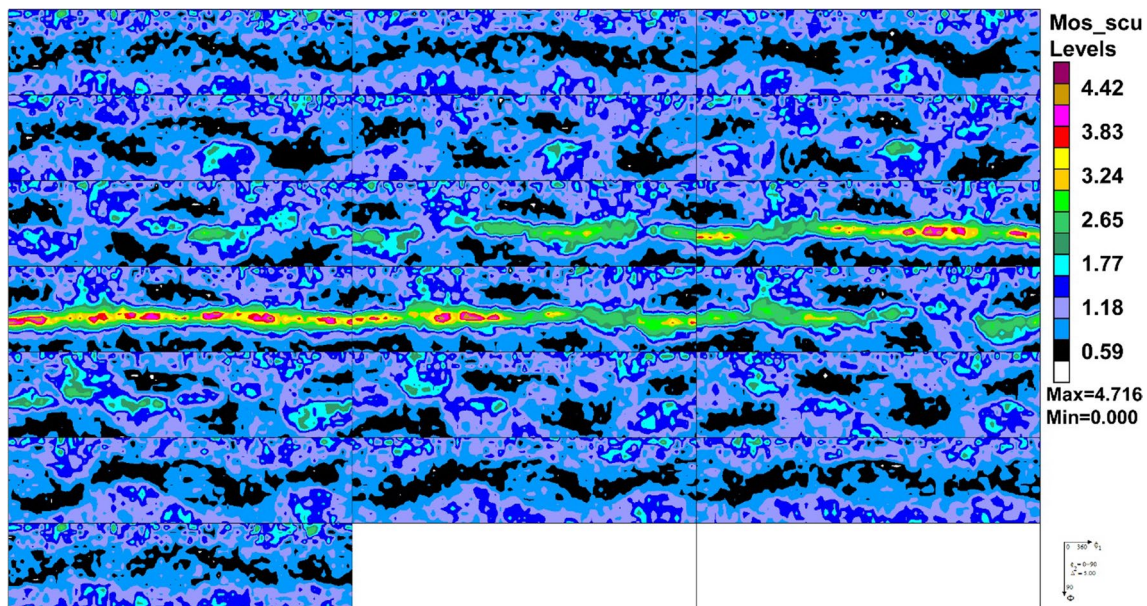


Fig. 1 Crystallographic texture (ODF), input wire

Fig. 2 The microstructure; starting wire, metallographic microscope (a) and surface image, SEM, secondary-electrons (b)

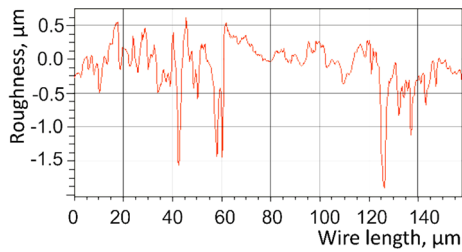
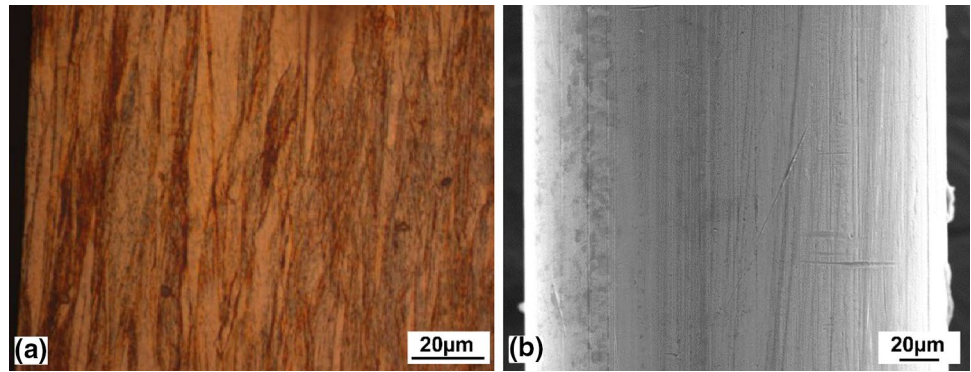


Fig. 3 The roughness of the input wire

In our wire texture, the component [100] was almost completely absent what can be associated with a relatively large amount of cold deformation. Such crystallographic texture in the DD process can cause the appearance of strain-induced roughness.

2.2 Methods

2.2.1 Conventional dieless drawing and multi-pass dieless drawing

The schematic and general view of the setup used in the experiment is shown in Fig. 4a and b, respectively. Bobbins [Fig. 4(4)] rotate at different speeds, providing the deformed wire velocities V_0 and V_1 ($V_1 > V_0$) by engines (5). The bobbins' speeds are controlled by dedicated PC software [Fig. 4(7)]. The engineering formula derived assuming constant volume was used to describe the wire longitudinal strain in a single pass:

$$\epsilon_{pass} = 1 - \frac{V_0}{V_1}. \tag{4}$$

An electric mini-furnace 20 mm long and 0.5 mm in diameter, was used as a heating device [Fig. 4(2)], but our setup allows alternative use of a laser [Fig. 4(8)] or an induction heater. Support rollers [Fig. 4(3)] were used for mechanical stabilization of deformed wire [Fig. 4(1)].

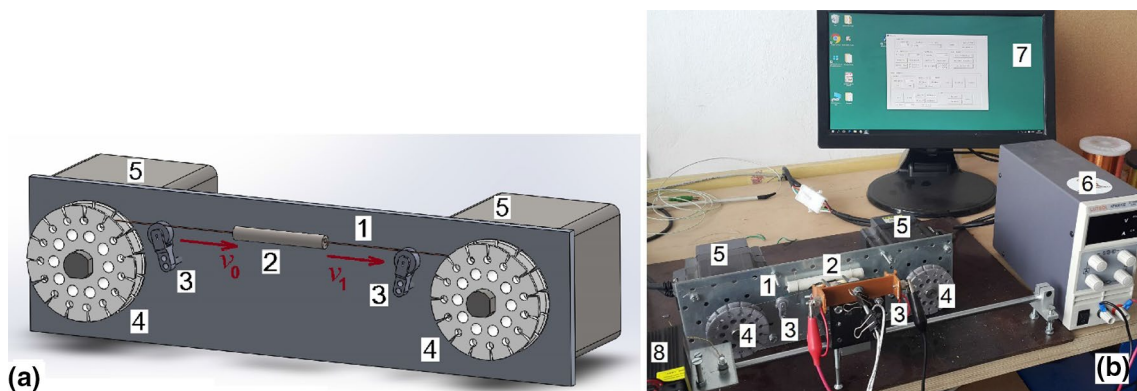


Fig. 4 Scheme a and general view of the setup b: 1—wire; 2—electrical heating device; 3—support rollers; 4—bobbins; 5—engines; 6—power supply for the electrical heating device; 7—a computer

with software for the process control; 8—alternative laser heating device (in the waiting position)

The paper explores two processes. Conventional one-pass DD is the first one. In this process, the velocity V_1 monotonically increased until the wire broke. In such a way, the maximum strain of the wire can be determined for given conditions.

The second process was MPDD. To carry out MPDD, at precise times, the bobbins' rotation direction is reversed, according to the number of passes. In this experiment, every single pass was similar to a DD process; however, the amount of strain in each pass was much smaller, corresponding to the one required for the process stability, and the strain was the same for each pass. The passes were repeated many times by changing the bobbins' rotation direction and speeds until the wire breaks. For both processes, the minimum diameter of the final product corresponds to the maximum workability.

2.2.2 Plastometry

The correct relationship between the flow stress and the strain, strain rate, and temperature is of key importance to assessing the stability of deformation during DD and MPDD. In the present study, the Hensel–Spittel equation was used as the flow stress model [26]:

$$\sigma = A e^{m_1 t} \epsilon^{m_2} \dot{\epsilon}^{m_3} e^{m_4/\epsilon} (1 + \epsilon)^{m_5} e^{m_6 \epsilon} \xi^{m_7} t^{m_8}, \tag{5}$$

where A, m_1 – m_8 —empirical coefficients; its values were experimentally determined from the results of the compression tests.

The test parameters covered temperature and the strain rate range of 400–650 °C and 0.3–1 s⁻¹, respectively. At least three samples with a diameter of 4 mm and a height of 6 mm, which were cut from an extruded rod, were used for each point of the measurement grid. The compression tests have been performed on a Zwick250 machine. A graphite-based MOLYKOTE P-37 Thread Paste, recommended for high-temperature plastometric compression tests, was used as a lubricant. The raw experimental data (i.e., the force vs. displacement) were processed using the inverse technique [27]. In this technique, empirical coefficients of the Eq. (5) were fitted in such a way that the differences (δ) between the calculated (P_{calc}) and the measured (P_{exper}) force were minimal:

$$\delta = \sum_{j=1}^k \sum_{i=1}^n (P_{exper} - P_{calc}(A, m_1, m_2 \dots m_8))^2, \tag{6}$$

where k is the sample number and n is the number of measurement points in one sample.

The procedure is described in detail elsewhere [28].

Following coefficients of Eq. (5) have been found as a result of the inverse analysis of the plastometric tests:

$A = 81,259.14, m_1 = -0.004279279, m_2 = 0.09383521, m_3 = -0.03657546, m_4 = -0.004250721, m_5 = 6.06186E-05, m_6 = -0.4821499, m_7 = 0.000317437, m_8 = -0.596443559$. A comparison of the experimental data and the recalculated ones is shown in Fig. 5 (thin solid lines and thick dot/dashed lines, respectively). The medium standard deviation is equal to 4.8% and its maximum value for all curves is equal to 9.2% only. The above coefficients were used to determine the stress–strain relationships shown in Fig. 6.

2.2.3 Finite element simulation

The commercial QForm software was used for the finite element (FE) simulation. Theoretical basis and examples of this software applications have been described by Biba et al. [29]. For the present simulation, a model of the rigid-plastic incompressible body was chosen. Flow stress data were implemented in the form of Eq. (5). Model geometry (Fig. 7) exactly matches the experimental conditions and the heating device was assumed to be motionless. Kinematic boundary conditions were set. On the ends of the wire, the velocities V_0 and V_1 were imposed. The K parameter value was calculated in every node of the FE grid at each time step by Eq. (2). To do this, a special script has been written in the LUA language [30]. The following boundary conditions were assumed in the simulation. The heat transfer coefficient in the heating device was 250 W/m² °C; in air 120 W/m² °C. The data were taken from the Qform database. The air temperature was 20 °C, the heating device temperature was set following the results of measurements by thermocouple and

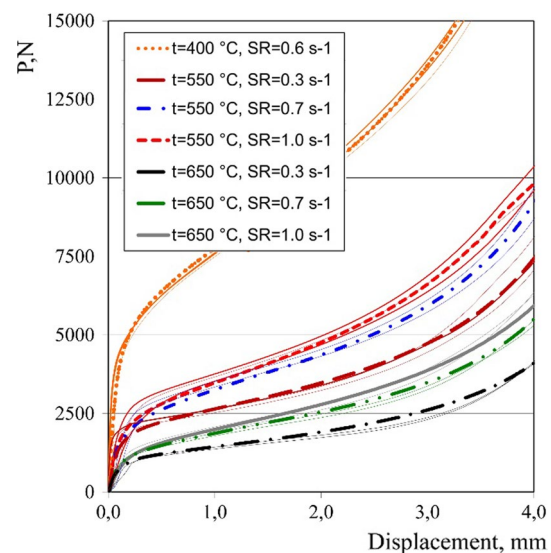


Fig. 5 Dependence of the load (P) during plastometric compressive tests of the CuZn37 alloy sample on the tool displacement: thin solid lines—experimental values; thick dashed lines—the ones calculated based on the FE simulation results; SR strain rate

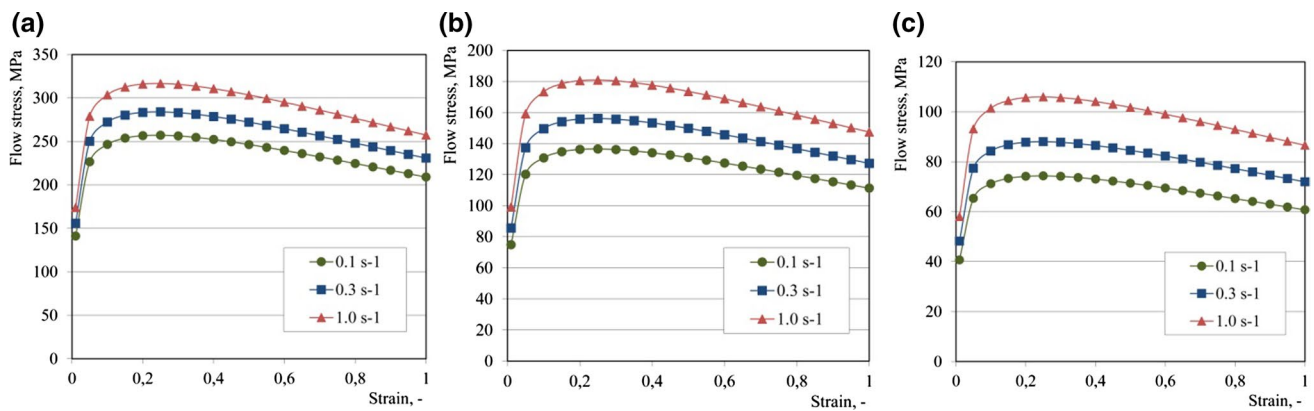


Fig. 6 The flow stress of the CuZn37 alloy for selected strain rates and temperatures: 400 °C (a), 500 °C (b), 600 °C (c)



Fig. 7 FE model of the process used in the Qform program, processed wire (1), a heating device (2)

was 400 °C. Kinematic conditions (velocities V_0 and V_1) were set under the experimental conditions.

3 Results and discussion

Illustrative relationship of the K parameter vs. strain, for the deformation temperature and strain rate equal to 400 °C and 0.1 s^{-1} , respectively, is shown in Fig. 8. This figure allows to estimate approximately the amount of strain up to which the process of simple stretching is stable ($K = 1$ corresponds to a strain of 0.07). However, as described above, this value cannot be directly used to assess the stability of the DD and MPDD processes due to the differences between simple stretching and DD. A more adequate estimate requires FE modeling.

Selected results of the FE simulation and experiments for DD and 8–16 passes of the MPDD one are collected in Table 1 and Figs. 9, 10, 11, 12, 13. Typical distributions of the K parameter along the deformed wire are shown in Fig. 9 for the DD (a, c) and MPDD (d) processes. The neck

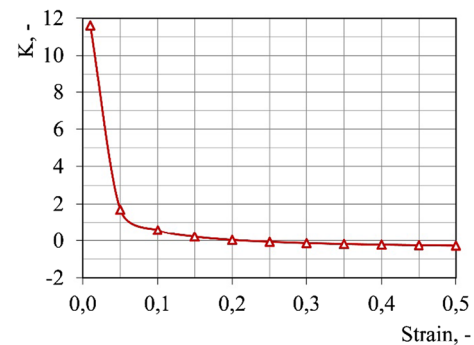


Fig. 8 Illustrative relationship of the parameter K vs. strain, for the deformation temperature and strain rate equal to 400 °C, and 0.1 s^{-1} , respectively

development up to the wire fracture corresponding to values of $K < 1$ as can be seen for the DD process (Fig. 9c). Cup and cone tensile fracture formed for this sample, shown in Fig. 10, is typical for the ductile metals. On the other hand, the stability of the MPDD process is evident ($K \gg 1$) (Fig. 9d).

The temperature dependence of the workability in DD process turned out to be non-monotonic (Table 1, variants no. 1–4). Generally, the ductility of copper and its alloys shows the intermediate temperature embrittlement (ductility trough behavior). This feature lies in the non-monotonic part of the ductility vs. temperature dependence. E.g., copper alloys ductility determined in tensile tests dramatically decreases with increasing temperature from 42.6% in 20 °C to 0.7% in 500 °C for CuCo2Be alloy, see table 2 in Ref. [31]. This effect is related to intergranular segregation of alloying additions or impurities [18]. A similar effect was observed by us during DD of the CuZn37 alloy when the temperature raised above 400 °C (Table 1, lines 3–6). In that case, the fracture mechanism occurs precisely along grain boundaries (Fig. 11), in accordance with the above concept.

Table 1 Selected results of the FE simulation and experiments

Experiment no.	V_0 , mm/s	V_1 , mm/s	ϵ_{pass}	n	d_{final} , mm	t_d , °C	t_{FEM} , °C	ϵ_{final}	E
1	12.16	14.7	0.173	1	0.184	300	262	0.167	–
2	12.16	18.1	0.328	1	0.170	400	347	0.325	–
3	12.16	16.7	0.272	1	0.175	500	437	0.267	–
4	12.16	18.2	0.332	1	0.170	600	531	0.325	–
5	12.16	13.38	0.091	8	0.137	400	351	0.757	2.33
6	12.16	12.77	0.048	16	0.136	400	353	0.771	2.37

In Table 1, V_0 , V_1 wire velocities during DD and MPDD, ϵ_{pass} longitudinal strain, calculated by Eq. (4), n number of MPDD passes, d_{final} final diameter of wire before fracture, t_d the temperature in the heating device, measured by thermocouple, t_{FEM} maximal temperature of wire in the deformation zone, calculated by FE model, ϵ_{final} final longitudinal strain, calculated using value d_{final} and equation $\epsilon_{final} = -2\ln(d_{final}/d_0)$; E —process efficiency calculated using equation $E = \epsilon_{final_MPDD} / \epsilon_{final_DD}$

Fig. 9 Selected results of the FE simulation: **a, b, c**—DD, Table 1 variant no. 2; **d, e**—MPDD, first pass, Table 1, variant no. 5; **a, c, d**—distribution of K value in the deformation zone; **b, e** distribution of longitudinal strain; **c** neck formation for $V_1 > 18.1$ mm/s, distribution of K value

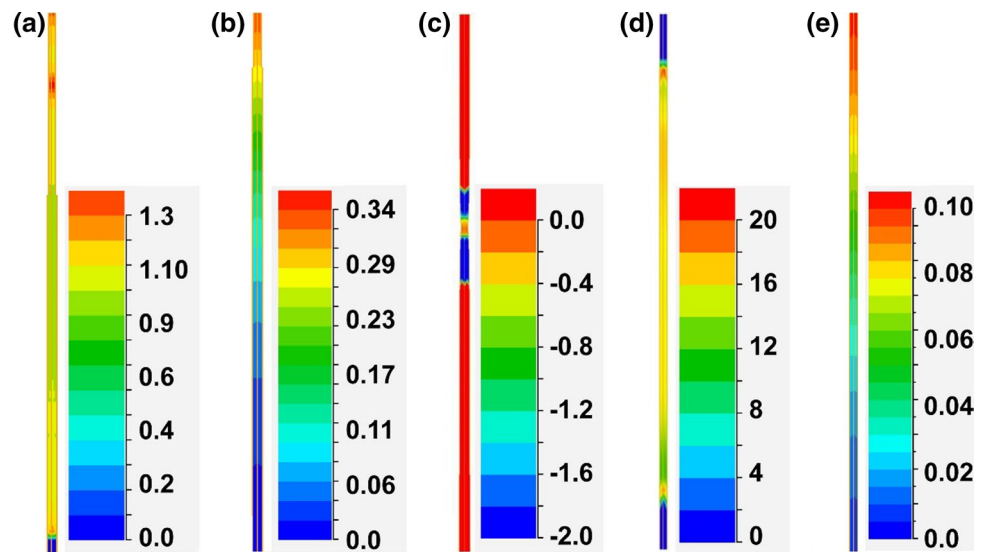
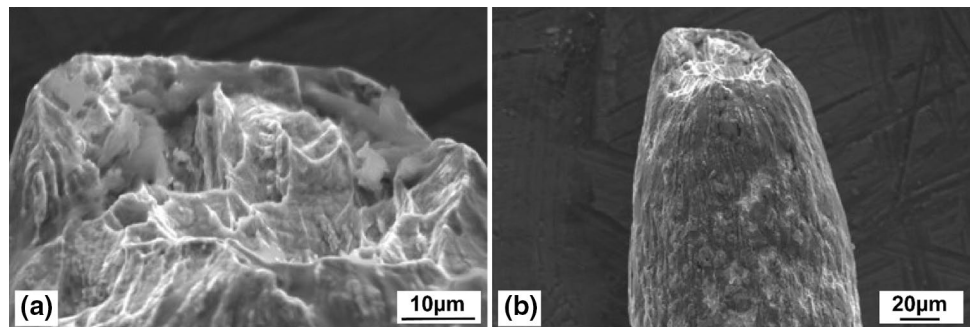


Fig. 10 Cup **a** and cone **b** tensile fracture, DD wire processed according to variant no. 2 from Table 1, SEM secondary-electron image



Thus, nearly the same workability was found for temperatures of 400 and 600 °C, and for other temperatures the values were significantly lower. For an industrial process, a temperature of 400 °C can be recommended, since an increase in the temperature accelerates oxidation of the surface. Therefore, a temperature of 400 °C was chosen also for the MPDD process performed with a significantly different partial longitudinal strain i.e., 0.091 (Table 1, variant

no. 5) and 0.048 (Table 1, variant no. 6). For both cases, the increase in the final longitudinal strain to wire breakage was more than double that of the DD process (Table 1, variant no. 2). The improvement in the workability of the material during MPDD (compare variants 2 and 5 in Table 1) is directly related to an increase in the stability of plastic deformation, which quantitatively corresponds to higher values of the parameter K (Fig. 9a and d). At large values of K , the

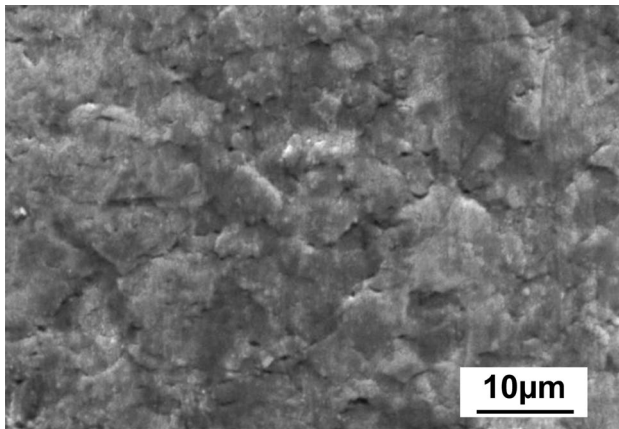


Fig. 11 Grain boundaries microcracks, the heating device temperature of 500 °C, line 3 in Table 1 (drawing direction is along the vertical axis)

localization of the deformation in the form of a neck is suppressed, which increases the maximum possible elongation of the workpiece (increase of workability).

Surprisingly, tool marks typical for the starting wire surface almost completely disappeared after DD (Figs. 2b and 12) and the surface image of the DD and MPDD processing wire is very similar (Fig. 12a and b). However, DD significantly increased surface roughness (Figs. 3, 13). Such an effect is induced by a non-constrained strain of the subsurface grains and can cause significant difficulties during the application of the DD and MPDD for the manufacturing of the extremely thin wire.

To study the dependence of roughness on temperature, additional DD experiments were carried out, in which the temperature conditions for variants 1–4 from Table 1 were repeated. The differences with the data in Table 1 were associated with the final deformation—for all temperatures, the final longitudinal strain was 0.17. The results of this experiment showed that an increase in the DD temperature leads to an increase in the product surface roughness. Illustrative results are shown in Fig. 14a. For DD processing of wires up to the same strain of 0.17, the greatest increase in the roughness was registered for the temperature of the wire in

Fig. 12 The surface of the wire after DD (a) and MPDD (b), Table 1, variants nos. 2 and 5, respectively; SEM secondary-electron images

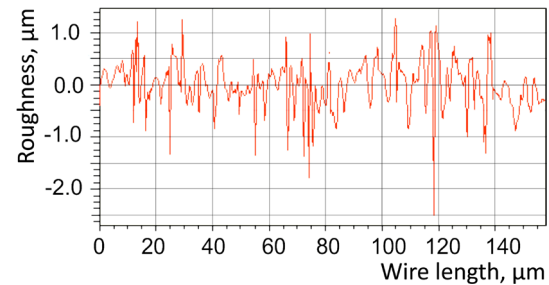
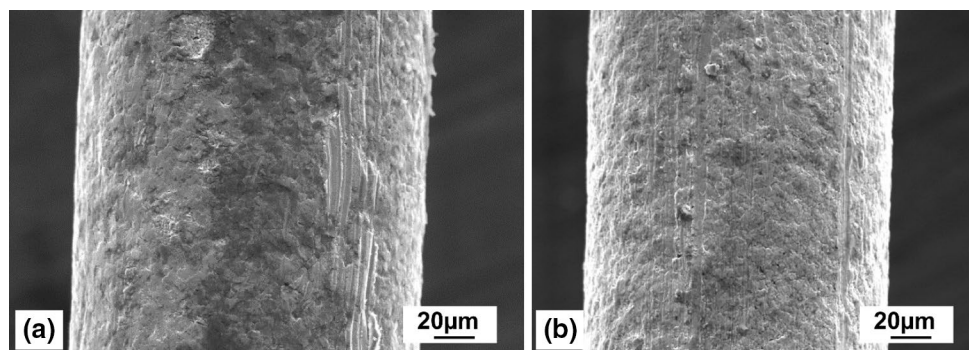


Fig. 13 The typical roughness of the wire after MPDD

the deformation zone of 262–347 °C, which corresponded to temperatures in the heating device 300–400 °C (Fig. 14a). Further, the increase of the roughness slows down.

The study of the dependence of roughness on longitudinal strain also required a repetition of the DD and MPDD experiments with sampling at each strain value. Measured roughness versus temperature and longitudinal strain is shown in Fig. 14b. Each point in this figure corresponds to a different DD or MPDD experiment. The statistical measurement error was obtained by performing three roughness measurements on each sample. The degree of longitudinal strain was determined by measuring the final diameter of the wire after processing and then calculating it using an engineering formula $\varepsilon_{final} = 2 \ln(d_{final}/d_0)$.

The roughness of MPDD processed wires seems to be a little lower than that of the DD ones, after similar deformation imposed at the same temperature (Fig. 14a and b). To the best of our knowledge, some decrease in roughness during MPDD was for the first time reported by Furushima et al. [32]. Their explanation of this phenomenon based on an empirical relationship describing the stretching effect of the roughness due to large elongation of the sample [33]. However, such an explanation does not answer the question why, with the same elongation, the roughness of the wire after MPDD is lesser than after the conventional process. In our opinion, the use of MPDD under conditions of high stability of plastic deformation reduces local differences in the product diameter along its length, which results in a reduction of roughness, as it was shown in Ref.

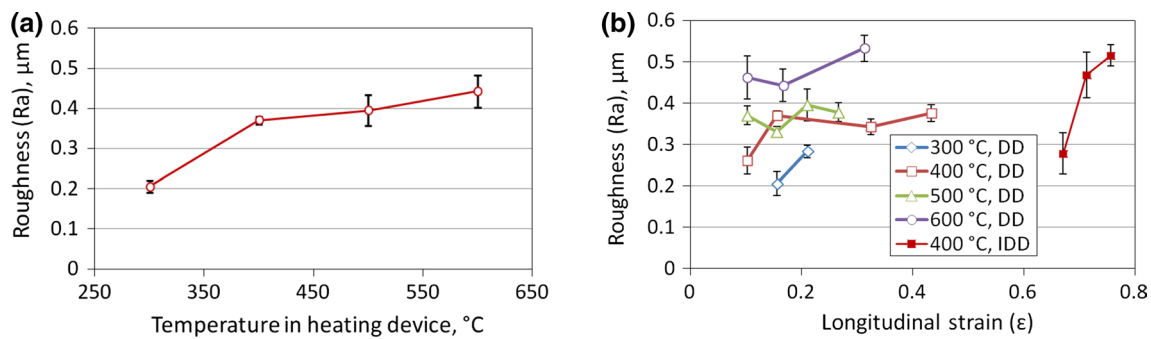


Fig. 14 The roughness of the final wire surface: DD, elongation 0.17 (a), MPDD (b)

[14]. However, a detailed proof of this statement is beyond the scope of the present study. Thus, this effect may be related to the differences in the strain distribution on the wire cross-section and will be addressed in future studies.

4 Conclusions

1. More than two times higher workability was observed for the multi-pass dieless drawing of the CuZn37 brass wire with the initial diameter of 0.2 mm to the final diameter of 0.14–0.18 mm in comparison with the conventional one-pass dieless drawing process. This effect was related to significantly higher stability of the deformation during the multi-pass drawing process.
2. No evident effect of the dieless drawing temperature on the workability was found, regarding the temperature from the technological window of the process. On the other hand, an increase in the temperature results in an increase in the product surface roughness.
3. When using multi-pass dieless drawing, the roughness of the final wire is comparable or less than the roughness after the conventional process. Considering that the multi-pass dieless drawing allows achieving a significantly greater longitudinal strain of the wire, this means that the new process not only increases the workability but also inhibits the development of the strain-induced surface roughness of the final wire.
4. The optimal parameters of the multi-pass dieless drawing process of the thin CuZn37 brass wire were as follows: the temperature of the heating device equal to 400 °C (which in turn results in the temperature of 347 °C of the material in the deformation zone), the deformation increment per pass is 0.048–0.09, the initial and final wire speeds in the experimental setup of 12.6 mm/s and 12.77–13.38 mm/s, respectively.

Funding The work was supported by the National Science Centre of Poland, Project No. 2017/27/B/ST8/01471.

Data availability Data are available.

Code availability Not applicable.

Declarations

Conflict of interest

The authors have no relevant financial or non-financial interests to disclose.

The authors have no conflicts of interest to declare that are relevant to the content of this article.

All authors certify that they have no affiliations with or involvement in any organization or entity with any.

Financial interest or non-financial interest in the subject matter or materials discussed in this manuscript.

The authors have no financial or proprietary interests in any material discussed in this article.

This paper does not contain any studies with human participants or animals performed by any of the authors.

Ethical approval Not applicable.

Consent for publication All authors agree to publish.

Open Access This article is licensed under a Creative Commons Attribution 4.0 International License, which permits use, sharing, adaptation, distribution and reproduction in any medium or format, as long as you give appropriate credit to the original author(s) and the source, provide a link to the Creative Commons licence, and indicate if changes were made. The images or other third party material in this article are included in the article's Creative Commons licence, unless indicated otherwise in a credit line to the material. If material is not included in the article's Creative Commons licence and your intended use is not permitted by statutory regulation or exceeds the permitted use, you will need to obtain permission directly from the copyright holder. To view a copy of this licence, visit <http://creativecommons.org/licenses/by/4.0/>.

References

- Singh J, Singh R, Kumar R. Review on effects of process parameters in wire cut EDM and wire electrode development. *Int J Innov Res Sci Technol*. 2016;2:701–6.
- Jewelry wire:everything you need to know, (n.d.). <https://door4studios.com/jewelry-wire-everything-you-need-to-know-to-make-the-best-choice/> Accessed 8 May 2021.
- Kraft FB. Three fine wire drawing systems – an economic comparison. *Wire J*. 1980;19:103–5.
- Weiss V, Kot RA. Dieless wire drawing with transformation plasticity. *Wire J*. 1969;9:182–9.
- Supriadi S, Furushima T, Manabe K-I. Development of precision profile control system with fuzzy model and correction function for tube dieless drawing. *J Solid Mech Mater Eng*. 2011;5:1059–70. <https://doi.org/10.1299/jmmp.5.1059>.
- Li K, Wang Z, Liu X. Study of deformation stability during semi-dieless drawing of Ti-6Al-4V alloy wire. *Materials (Basel)*. 2019. <https://doi.org/10.3390/ma12081320>.
- Tiernan P, Hillery MT. Dieless wire drawing - An experimental and numerical analysis. *J Mater Process Technol*. 2004;155–156:1178–83. <https://doi.org/10.1016/j.jmatprotec.2004.04.175>.
- Li Y, Quick NR, Kar A. Dieless laser drawing of fine metal wires. *J Mater Process Technol*. 2002;123:451–8. [https://doi.org/10.1016/S0924-0136\(02\)00110-3](https://doi.org/10.1016/S0924-0136(02)00110-3).
- Milenin A. Rheology-based approach of design the dieless drawing processes. *Arch Civ Mech Eng*. 2018;18:1309–17. <https://doi.org/10.1016/j.acme.2018.04.003>.
- Considère A. Mémoire sur l'emploi du fer et de l'acier dans les constructions. *Ann Des Ponts Chaussées*. 1885;34:574–95.
- Slomchack GD, Milenin AA, Mamuzić I, Vodopivec F. A mathematical model of the formation of the plastic deformation zone in the rolling of rheologically complex metals and alloys. *J Mater Process Technol*. 1996;58:184–8. [https://doi.org/10.1016/0924-0136\(95\)02099-3](https://doi.org/10.1016/0924-0136(95)02099-3).
- Bylya OI, Khismatullin T, Blackwell P, Vasin RA. The effect of elasto-plastic properties of materials on their formability by flow forming. *J Mater Process Technol*. 2018;252:34–44. <https://doi.org/10.1016/j.jmatprotec.2017.09.007>.
- Soboyejo WO. *Mechanical properties of engineered materials*. New York: Marcel Dekker; 2003.
- Y.G. Li, *Laser Micro-processing and thermomechanical modeling of plasticity for dieless wire drawing*, doctoral dissertation 1591, University of Central Florida. 2002. <https://stars.library.ucf.edu/rtd/1591/>
- He Y, Liu X, Xie J, Zhang H. Processing limit maps for the stable deformation of dieless drawing. *Int J Miner Metall Mater*. 2011;18:330. <https://doi.org/10.1007/s12613-011-0443-8>.
- Milenin A, Furushima T, Du P, Pidvysots'kyi V. Improving the workability of materials during the dieless drawing processes by multi-pass incremental deformation. *Arch Civ Mech Eng*. 2020. <https://doi.org/10.1007/s43452-020-00092-4>.
- Wright RN, Wright EA. Basic analysis of dieless drawing. *Wire J Int*. 2000;33:138–43.
- Laporte V, Mortensen A. Intermediate temperature embrittlement of copper alloys. *Int Mater Rev*. 2009;54:94–116. <https://doi.org/10.1179/174328009X392967>.
- Furushima T, Manabe K. Dieless drawing process of extruded non-circular aluminum alloy tubes with double hollow section. *J Jpn Inst Light Met*. 2007;57:351–6. <https://doi.org/10.2464/jilm.57.351>.
- Furushima T, Imagawa Y, Manabe KI, Sakai T. Effects of oxidation and surface roughening on drawing limit in dieless drawing process of SUS304 stainless steel microtubes. *J Mater Process Technol*. 2015;223:186–92. <https://doi.org/10.1016/j.jmatprotec.2015.03.033>.
- Milenin A, Furushima T, Němeček J. Transformation of surface roughness of mg alloy tubes during laser dieless drawing. *J Mater Eng Perform*. 2020;29:7736–43. <https://doi.org/10.1007/s11665-020-05234-6>.
- Milenin A, Byrska-Wójcik D, Wróbel M. Physical modelling of strain induced roughness of copper wire during dieless drawing process. *Mater Sci Forum*. 2021;1016:900–5.
- The Texture Analysis Software for Windows, (n.d.). <http://www.labosoft.com.pl> Accessed 8 May 2021.
- Schulz LG. A direct method of determining preferred orientation of a flat reflection sample using a Geiger counter x-ray spectrometer. *J Appl Phys*. 1949;20:1030–3. <https://doi.org/10.1063/1.1698268>.
- Stout MG, O'Rourke JA. Experimental deformation textures of OFE copper and 70:30 brass from wire drawing, compression, and torsion. *Metall Trans A*. 1989;20:125–31. <https://doi.org/10.1007/BF02647499>.
- Hansel A, Spittel T. *Kraft- und arbeitsbedarf bildsamer formgebungsverfahren*. Lipsk: VEB Deutscher Verlag für Grundstoffindustrie; 1978.
- Szeliga D, Pietrzyk M. Testing of the inverse software for identification of rheological models of materials subjected to plastic deformation. *Arch Civ Mech Eng*. 2007;7:35–52. [https://doi.org/10.1016/S1644-9665\(12\)60003-X](https://doi.org/10.1016/S1644-9665(12)60003-X).
- A. Milenin, P. Kustra, J.-M. Seitz, F.-W. Bach, D. Bormann, Production of thin wires of magnesium alloys for surgical applications, in: 2010 Conf. Proc. Wire Assoc. Int. Inc. - Wire Cable Tech. Symp. 80th Annu. Conv. 2010.
- N. Biba, A. Maximov, S. Stebunov, A. Vlasov, The model for simulation of thermally, mechanically and physically coupled problems of metal forming, in: D.S. J. Kusiak, J. Majta (Ed.), Proc. 14th Int. Conf. Met. Form., Kraków. 2012: pp. 1363–1366.
- The programming language Lua. 2021. <http://www.lua.org/> Accessed 8 May 2021.
- Ozgowicz W, Grzegorzczak B. The influence of the temperature of plastic deformation on the structure and mechanical properties of copper alloys CuCo2Be and CuCo1Ni1Be. *Arch Mater Sci Eng*. 2009;39(1):5–12.
- Furushima T, Manabe K. Experimental study on multi-pass dieless drawing process of superplastic Zn–22%Al alloy microtubes. *J Mater Process Tech*. 2007;187–188:236–40. <https://doi.org/10.1016/j.jmatprotec.2006.11.204>.
- Osakada K, Oyane M. On the roughening of free surface in deformation processes. *Bull JSME*. 1971;14:171–7. <https://doi.org/10.1299/jsme1958.14.171>.

Publisher's Note Springer Nature remains neutral with regard to jurisdictional claims in published maps and institutional affiliations